FD-MMAC: Combating Multi-Channel Hidden and Exposed Terminals Using a Single Transceiver

Yan Zhang, Loukas Lazos, Kai Chen, Bocan Hu, and Swetha Shivaramaiah
Dept. of Electrical and Computer Engineering, University of Arizona
Email: {yanzhang, llazos, chenkai, bocanhu, sshivaramaiah}@email.arizona.edu

***Abstract*—We address the problem of improving the throughput and delay efficiency of distributed multi-channel MAC (MMAC) protocols. We design an MMAC protocol called FD-MMAC that exploits recent advances in full-duplex (FD) communications to coordinate channel access in a distributed manner. Compared with prior MMAC designs, the FD-MMAC protocol eliminates the use of in-band or out-of-band control channels for combating the multi-channel hidden terminal problem, discovering the resident channel of destinations, and performing load balancing. Furthermore, FD-MMAC improves the spectral efficiency by enabling the operation of multi-channel exposed terminals. To achieve its goals, FD-MMAC integrates an advanced suite of PHY-layer techniques, including self interference suppression, error vector magnitude and received power measurements, and signal correlation techniques. We validate the proposed PHY-layer techniques on NI USRP devices. Further, we show via simulations that FD-MMAC achieves significantly higher throughput and lower delay compared with prior art.**

I. Introduction

The delay and throughput performance of wireless networks can be significantly improved by accommodating parallel transmissions over orthogonal frequency bands. Most wireless standards (e.g., [1]) already provision for multiple bands, herein referred to as *channels*. For networks without centralized control, channel access is coordinated in a distributed fashion by the medium access control layer (MAC), using a multi-channel MAC (MMAC) protocol [2]–[7].

The design of MMAC protocols poses significant challenges. Senders must employ low-overhead mechanisms for discovering the resident channel of their respective destinations. Moreover, parallel transmissions must be efficiently distributed over all available channels to balance the traffic load and alleviate contention. The latter is a complicated process due to the multi-channel hidden terminal problem [3]. In this problem, a sender that switches to a busy channel is unable to detect an ongoing transmission if it is a hidden terminal to the transmitter. Current solutions to the multi-channel hidden terminal problem incur significant control overhead by requiring the use of in-band or out-of-band control channels [2]–[5], or the availability of multiple transceivers per device [6], [8], [9]. Finally, most existing MMAC protocols fail to address the multi-channel exposed terminal problem [10], whereby a sender switching to a busy channel, but being an exposed terminal to a transmitter, cannot proceed with a parallel non-interfering transmission.

978-1-4799-3360-0/14/$31.00

To improve the spectral efficiency of MMAC protocols, we exploit recent advances in full-duplex (FD) communications over a *single* channel [11]–[14]. In certain low-power wireless environments, sophisticated self interference suppression (SIS) techniques allow for concurrent transmission and reception over a single channel. This is achieved by suppressing a significant portion of the self interference (up to 80 dB), using a combination of antenna-based SIS [14], signal inversion [12], RF and digital interference cancellation [13], [15]. The integration of FD communications in the MMAC design provides unique opportunities for reducing the control overhead and increasing the spatial channel reuse. In this paper, *we address the problem of improving the throughput and delay efficiency of MMAC protocols, when nodes can operate in FD mode*.

Our Contributions–We design an MMAC protocol called FD-MMAC that enables distributed coordination of channel access over orthogonal channels for devices using a single transceiver. Compared with prior MMAC designs, the FD-MMAC protocol provides the following attractive features.

- It eliminates in-band and out-of-band control signaling for combating the multi-channel hidden terminal problem, discovering the resident channel of destinations, and performing load balancing.
- It increases the spatial channel reuse by enabling the operation of multi-channel exposed terminals.
- It achieves load balancing and fairness autonomously.

Though security considerations are beyond the scope of the present work, FD-MMAC is less vulnerable to denial-of-service attacks launched against the control channel [16], [17], due to the elimination of signaling on a dedicated control band. To achieve its goals, FD-MMAC integrates an advanced suite of PHY-layer techniques, including SIS, error vector magnitude (EVM) and received power measurements, and signal correlation techniques. We validate these PHY-layer techniques on an NI USRP testbed. Further, we show via packet-level simulations that FD-MMAC achieves significantly higher throughput and lower delay compared with prior art. To the best of our knowledge, this is the first work to propose an MMAC protocol design that exploits the FD communication mode.

Paper Organization–In Section II, we motivate our problem by discussing the limitations of related work. The system model is described in Section III. Section IV describes the FD carrier sensing operation. In Section V, we address the multi-channel hidden and exposed terminal problems. In Section VI, we

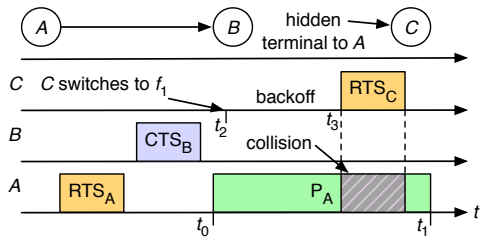

Fig. 1. The multi-channel hidden terminal problem.

present the operational details of FD-MMAC. We compare the performance of FD-MMAC with existing MMAC designs in Section VII and conclude in Section VIII.

II. Motivation - Related Work

MMAC protocols can be broadly categorized to three classes: (a) split-phase [3], [5], [18], (b) dedicated control channel (DCC) [6]–[10], and (c) rendezvous [2], [19]. In split-phase MMACs, time is divided to alternating control and data phases. During the control phase, all nodes converge to a default channel to negotiate the channel assignment for the upcoming data phase using a variant of the virtual carrier sensing mechanism [1]. During the data phase, nodes exchange data on the assigned channels. In DCC MMACs, nodes are equipped with two radios. One radio is always tuned to a DCC to perform channel assignment and virtual carrier sensing. The second radio switches between the remaining channels to perform data transmissions. Finally, in rendezvous protocols, nodes hop between channels using predefined hopping sequences. These sequences are designed to enable the sender-destination rendezvous within a fixed time period. We now motivate our work by highlighting the limitations of existing MMACs.

The multi-channel hidden terminal problem: We first describe the multi-channel hidden terminal problem using the topology of Fig. 1. Let nodes A and B reside on channel f_1, while node C resides on f_2. Topologically, C is a hidden terminal to A. Assume that A performs an RTS-CTS exchange over f_1 (virtual carrier sensing enabled) before communicating packet P_A to B. Let the transmission of P_A start at time t_0 and terminate at t_1. Assume that C switches to f_1 at t_2 with $t_0 < t_2 < t_1$. Because $t_2 > t_0$, node C will not overhear the CTS$_B$. Moreover, because $t_2 < t_1$, the transmission of P_A is ongoing when C switches to f_1. At time $t_3 < t_1$, node C becomes active and causes a collision at B.

Split-phase MMACs avoid multi-channel hidden terminals by performing channel negotiations on a default control channel. Because all nodes reside on the default channel during the control phase, the virtual carrier sensing mechanism prevents hidden terminals. However, no data transmissions take place during the control phase, thus decreasing the overall spectral efficiency. The control phase can be considerably long under high-contention conditions. Moreover, when a sender has packets for multiple destinations, it may switch channels during a single data phase. In this case, a multi-channel hidden terminal can avoid collisions only if it defers from transmission for a period equal to the duration of the maximum transmission unit plus an ACK. This delay decreases the spectral efficiency.

In DCC MMACs, virtual carrier sensing is performed over the DCC. Because one radio is always tuned to this channel, nodes are aware of all scheduled data transmissions. Hence, multi-channel hidden terminals are avoided. However, the use of one extra radio increases the device cost. Moreover, the spectral efficiency is decreased by dedicating one channel for signaling. The capacity of the control channel becomes the performance bottleneck in high-contention scenarios. Finally, from a security standpoint, the control channel constitutes a single point of failure [16], [17]. Rendezvous protocols do not address the multi-channel hidden terminal problem.

The multi-channel exposed terminal problem: Multi-channel exposed terminals lose transmission opportunities when switching to a busy channel in the middle of a data transmission. Referring to Fig. 1, assume that B transmits a data packet to A on f_1 starting at t_0. Node C switches to f_1 at t_2 with $t_0 < t_2 < t_1$. Node C will sense the channel busy and defer from transmission, thus losing an opportunity to operate in parallel with the $B \rightarrow A$ transmission. Prior MMAC protocols solve the exposed terminal problem using additional radios and/or dedicated control channels [7], [10].

Destination discovery and load balancing: In a multi-channel setting, a destination must be discoverable by a candidate sender. Moreover, parallel communications must be distributed over all channels to balance the traffic load and alleviate contention. In DCC and split-phase MMAC protocols, these two functions are performed by exchanging control messages, thus decreasing the spectral efficiency. Rendezvous protocols incur less overhead for destination discovery, since a destination's hopping sequence can be known a priory. However, these protocols do not combat multi-channel hidden terminals. Moreover, in some designs, an initial discovery delay is incurred until the sender's and destination's hopping sequences overlap [2]. In FD-MMAC, destination discovery and load balancing are achieved without the exchange of control information. Nodes independently switch to idle channels by tracking the state of each channel.

III. System Model

Network model: We consider a wireless network that operates over a set of orthogonal channels, denoted by $\mathcal{F} = \{f_1, f_2, ..., f_n\}$. For simplicity, we assume that all channels have the same bandwidth and propagation characteristics. Nodes are equipped with a single radio transceiver and are assumed to be time-synchronized to a common slotted system. Time synchronization can be achieved using out-of-band solutions such as GPS [20], or any of the readily available in-band methods [21]. We note that time-slotted synchronization is not a necessary FD-MMAC requirement. It is assumed here to facilitate legacy operations used by FD-MMAC, such as the slotted CSMA algorithm. However, FD-MMAC can also operate in an asynchronous mode.

SIS and signal correlation: Nodes can operate in FD mode by applying a combination of analog and digital SIS techniques [11]–[14]. In FD mode, a node can receive while simultaneously transmitting over the same channel. Moreover,

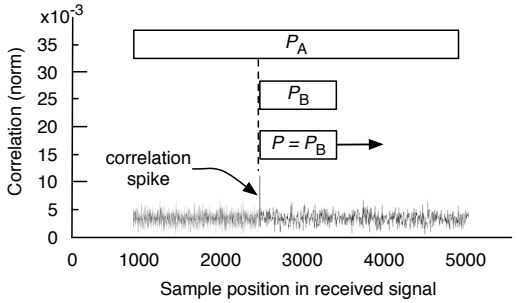

Fig. 2. Detecting a known bit pattern P when two packets collide using the signal correlation technique.

nodes can apply signal correlation techniques for detecting the transmission of known bit patterns. These techniques are common in frame detection, even in the presence of collisions [15]. The concept of signal correlation is shown in Fig. 2. Consider the concurrent reception of packets P_A and P_B at C. Node C is interested in detecting whether $P_B = P$, where P is a known bit pattern. Let the sampled signal representing P be $\mathcal{L}$ samples long. Node C computes the signal correlation value between $P_A + P_B + w$ and P (w denotes the noise component at the receiver) by aligning the $\mathcal{L}$ samples of P with the first $\mathcal{L}$ samples of $P_A + P_B + w$. It then shifts the alignment of P by one sample and recomputes the correlation until the end of $P_A + P_B + w$ is reached. Formally, let $x[i]$ denote the i^{th} sample of P and $y[j]$ the j^{th} sample of the received signal. The correlation value at the j^{th} sampled position of $y[j]$ is:

$$C[j] = \sum_{i=1}^{\mathcal{L}} x^*[i]y[j+i], \tag{1}$$

where $x^*[i]$ is the complex conjugate of $x[i]$. The correlation value will peak when P is aligned with P_B. Using this correlation method, node C can identify if P is transmitted, despite the concurrent transmission of P_A. In practice, node C must compensate $C[j]$ for the frequency offset of B. The frequency offset can be estimated in advance from prior packet exchanges between B and C. A limitation of signal correlation is that the known bit pattern has to exhibit desirable cross-correlation properties.

IV. FD Carrier Sensing

The carrier sensing function can be extended to the receiver's collision domain when that receiver operates in FD mode [12], [22]. We refer to this mechanism as *FD carrier sensing*. In FD-MMAC, we improve FD carrier sensing by integrating a suite of PHY-layer techniques. Our techniques extend beyond the estimation of the carrier state (idle or busy) and determine a node's operational state relative to an ongoing transmission. The state information is used to create transmission opportunities for exposed terminals, avoid collisions caused by hidden terminals, and discover the resident channel of a destination.

Operation in FD mode: The FD carrier sensing mechanism is shown in Fig. 3. A sender A initiates the transmission of P_A to B. Node B decodes the MAC header of P_A and determines it is the destination. Node B transmits a *beacon packet* BCN$_B$

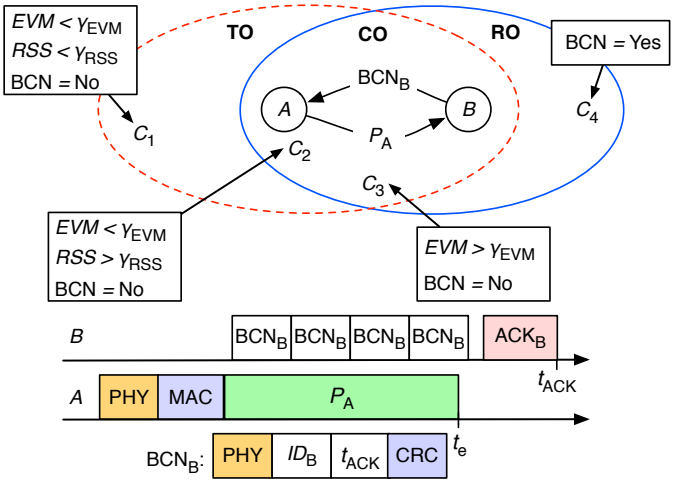

Table 1: Region Classification Rules

	BCN	$EVM < \gamma_{EVM}$	$RSS < \gamma_{RSS}$	Region
C_1	No	Yes	Yes	TO
C_2	No	Yes	No	CO
C_3	No	No	-	CO
C_4	Yes	-	-	RO

Fig. 3. The three regions for a node C relative to a data transmission $A \rightarrow B$.

while receiving P_A by operating in FD mode. This mechanism was demonstrated in [22] for a single channel MAC. Node A receives BCN$_B$ by also operating in FD mode. With the reception of BCN$_B$, node A verifies that B is receiving P_A and continues the transmission of P_A. Lack of a BCN reply implies either that B is unavailable (B is at another channel or a hidden terminal to another transmission) or that the MAC header of P_A got corrupted. Node A uses the lack of BCN$_B$ as an early collision detection mechanism and aborts the further transmission of P_A.

Generally, a data packet P is expected to be much longer than a BCN packet. To account for this difference, BCN packets are transmitted back-to-back until the reception of P is completed. The reception ending time t_e is known to the destination based on the network allocation vector (NAV) included in P's MAC header. The BCN contains the destination's id, the time slot t_{ACK} at which the ACK transmission is to be completed, and a CRC code. If the reception of P is successful, the destination replies with an acknowledgement (ACK).

Operation State Classification: To combat multi-channel hidden terminals and enable multi-channel exposed terminals, nodes that sense channel activity perform *region classification* to determine their operation state. We divide the collision domains of A and B to the three regions shown in Fig. 3: (a) the receiver-only (RO) region, (b) the collision region (CO), and (c) the transmitter-only (TO) region. Referring to Fig. 3, a node C can determine its region using the following rules.

1) If C can decode BCN$_B$, it infers that it is in the RO region (hidden terminal).
2) if C cannot decode the received signal due to the collision of P_A with BCN$_B$, it infers it is in the CO region.
3) If C can decode P_A, it infers that it is in the TO region

(exposed terminal).

If C concludes that it is located in the CO/RO regions, it defers from transmission to prevent a collision at B. Otherwise, it explores transmission opportunities as an exposed terminal.

Practical Issues: Several practical issues complicate the proposed region classification rules. First, when C is in the TO region (position C_1 in Fig. 3), it cannot verify the correct decoding of P_A until P_A's transmission is completed and the CRC code is checked. Similarly, if C switches to a busy channel in the middle of P_A's transmission, the CRC code cannot be checked. Both these scenarios eliminate exposed terminal transmission opportunities. To evaluate the decodability of P_A before the reception of the CRC code, node C computes the error vector magnitude (EVM) on the received symbols. The RMS EVM value (dB) is given by [23]:

$$EVM_{RMS}(dB) = 20\log\left(\sqrt{\frac{\frac{1}{n}\sum_{k=1}^{n}|s_k^t - s_k^r|^2}{\frac{1}{M}\sum_{i=1}^{M}|s_i|^2}}\right), \quad (2)$$

where s_k^t is the k^{th} transmitted symbol, s_k^r is the k^{th} received symbol, n is the window size (in symbols) over which the EVM is computed, s_i is the i^{th} constellation symbol, and M is the number of constellation symbols. The EVM serves as a measure of the signal quality and is strongly correlated to the bit error rate [23]. It characterizes the signal distortion due to impairments of the wireless channel and undesired interference.

Note that the s_k^ts corresponding to the received s_k^rs *are not known* to C for arbitrary packets. To compute the EVM using formula (2), node C selects those s_k^ts in the constellation diagram that are closest to the received s_k^rs. This is because when a packet is correctly decoded, it is expected that the received symbols are closest to the actual transmitted symbols (hence, the correct decoding). On the other hand, in a collision scenario, the received symbols have a large distance from the ideal symbols, yielding a larger EVM.

In our classification, we compute the EVM over the duration of two BCN packets. This is to differentiate between the TO and the RO regions, where nodes are expected to have a lower EVM compared with the CO region. If a node C is located in the RO region, it is likely to decode at least one BCN packet within two BCN packet durations (recall that C can switch to a busy channel at any time). Otherwise, if C is in the TO region, it will not decode a BCN packet, but will have a low EVM value. For the EVM classification rule, the EVM at C is compared with a threshold γ_{EVM}.

Low EVM values and undecodability of a BCN packet can also be recorded due to the capture effect [24], when C is in the CO region but very close to A (position C_2 in Fig. 3). In this case, a potential transmission by C will cause a collision at B. To prevent this collision, we incorporate received signal strength (RSS) measurements. If the RSS measurement at C is beyond a threshold γ_{RSS}, node C concludes that it is in the CO region, despite having a low EVM value. Finally, if C is in the CO region, but can decode the BCN due to its proximity to B, for all practical purposes we allow C to infer that it is in the RO region. This is because for both the CO and RO regions, C will defer from transmission. The region classification rules used by FD-MMAC are summarized in Table 1. In Section VII, we perform testbed experiments for determining γ_{EVM} and γ_{RSS} based on measurements at locations $C_1 \ldots C_4$.

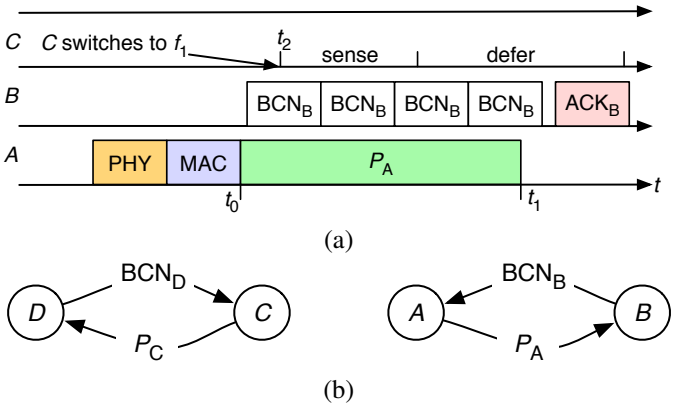

Fig. 4. (a) Combating the multi-channel hidden terminal problem, (b) exposed terminal operation. Transmission $C \rightarrow D$ occurs in parallel with transmission $A \rightarrow B$ on the same channel.

V. Combating Hidden and Exposed Terminals

FD carrier sensing eliminates the multi-channel hidden terminal problem. We illustrate this in Fig. 4(a) for the topology of Fig. 3, in which C is a hidden terminal to A. Node A transmits P_A to B over f_1 at time t_0. Node B decodes the PHY and MAC headers and infers that it is the destination. Node B replies with BCN$_B$ that is repeated for the duration of P_A, which terminates at t_1. Node C switches to f_1 at t_2 with $t_0 < t_2 < t_1$. First, C senses f_1 to be busy due to the BCN$_B$ transmissions. Second, C attempts to decode a BCN for two BCN durations. By decoding BCN$_B$, node C infers it is in the RO region and defers from transmission. If BCN$_B$ cannot be decoded, the EVM is expected to be high and hence, C will infer it is in the CO region and defer from transmission.

Early collision detection: A collision due to hidden terminals is still possible during the transmission of the PHY and MAC headers of P. Under a collision scenario, the destination will be unable to decode the MAC header and will not transmit a BCN packet. We use the absence of a BCN packet as an early collision detection mechanism. If the sender does not receive a BCN reply, it assumes that the attempted data transmission has collided or the destination is unavailable. The sender aborts further transmission of P and attempts retransmission without waiting for the expiration of the ACK timer.

Enabling Exposed Terminal Transmissions: An exposed terminal node C located in the TO region of an ongoing transmission $A \rightarrow B$ will attempt to communicate P_C to a candidate destination D. If D can decode the MAC header of P_C, it will respond with BCN$_D$ packets by operating in FD mode. Node C will continue the transmission of P_C if it detects BCN$_D$, and will abort otherwise. The destination D will not be able to respond with BCN$_D$ if one of the following occurs: (a) D is in the collision domain of another transmission and hence, cannot decode the MAC header of P_C or, (b) D

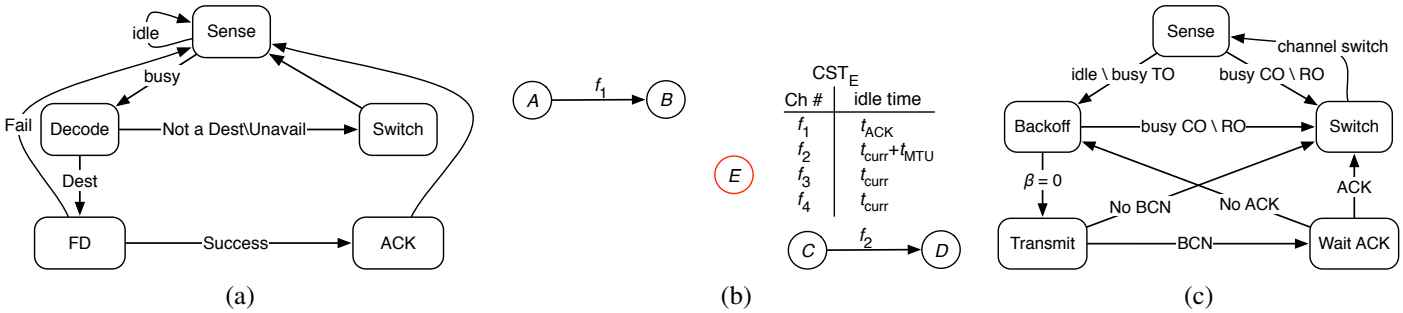

Fig. 5. (a) The state diagram of an FD-MMAC destination, (b) the CST table for node E, and (c) the state diagram of an FD-MMAC sender.

resides on another channel. The exposed terminal operation for transmissions $A \rightarrow B$ and $C \rightarrow D$ is shown in Fig. 4(b).

Receiving BCN/ACK packets in the presence of exposed terminals: Exposed terminal transmissions create two fundamental problems. First, nodes A and C cannot decode BCN_B and BCN_D, respectively, due to the interference they cause to each other. Similarly, nodes A and C cannot decode ACK_B and ACK_D, respectively, due to the interfering transmissions of P_C and P_A. To enable the concurrent operation of $A \rightarrow B$ and $C \rightarrow D$, we use the signal correlation technique for detecting known bit patterns [15].

Node C applies the signal correlation technique to detect BCN_D and ACK_D when P_A is concurrently transmitted. Similarly, node A applies the signal correlation technique to detect BCN_B and ACK_B when P_C is concurrently transmitted. Note that a node is aware of the exact composition of the BCN (ACK) packet and the approximate time that a BCN (ACK) is expected. Hence, it can limit the signal correlation within only a few sample shifts. One limitation here is that the BCN (ACK) has to exhibit desirable cross-correlation properties. Therefore, the BCN (ACK) is hashed (except the PHY header) with a uniform hash function to produce a random output.

VI. The FD-MMAC Protocol

FD-MMAC is a contention-based, time-slotted protocol based on CSMA/CA. To improve its spectral efficiency, FD-MMAC eliminates the message overhead related to virtual carrier sensing, destination discovery, and channel negotiation. The destination and sender state diagrams are shown in Fig. 5.

A. Destination Operation

When a node's transmission queue is empty, it operates as a destination. A destination selects a resident channel such that it can be discovered by candidate senders. Referring to the state diagram of Fig. 5(a), a destination operates as follows.

Sense state: In the "Sense" state, the destination continuously senses the resident channel. If the resident channel becomes busy, the destination transitions to the "Decode" state.

Decode state: In the "Decode" state, the destination attempts to decode the received signal. It transitions to the "FD" state if the MAC header is successfully decoded, the receiving node is the intended destination, and it is available for reception. Otherwise, it transitions to the "Switch" state.

FD state: In the "FD" state, the destination operates in FD mode. Based on the MAC header of P, the destination determines the t_{ACK} and the number of BCN packets that need to be transmitted. Then, it transmits BCN packets until the reception of P is completed. The destination checks the CRC code of P. If P is successfully received, it transitions to the "ACK" state. Otherwise, it returns to the "Sense" state.

ACK state: After a successful packet reception, the destination replies with an ACK and returns to the "Sense" state.

Switch state: In the "Switch" state, the destination autonomously determines its resident channel. This decision is based on a *channel state table (CST)* that records the expected time that each channel becomes idle (*idle time*). The CST is updated in the following way:

1) If the resident channel f_i is idle, set the idle time for f_i to the current slot t_{curr}.
2) If the resident channel f_i is busy and the destination is the RO region (BCN is decodable), set the idle time for f_i to t_{ACK} (contained in the BCN).
3) If the resident channel f_i is busy and the destination is in the CO/TO region (BCN not decodable), set the idle time for f_i to $t_{curr} + T_{MTU}$, where T_{MTU} is the transmission duration of the maximum transmission unit (MTU) packet plus the corresponding ACK.

After the CST update, the destination switches to the channel with the earliest idle time. In the case of ties, the current resident channel is preferred to avoid unnecessary channel switches. Otherwise, ties are broken arbitrarily. The proposed switching mechanism achieves several desirable properties. First, a destination waits for a candidate sender on the channel with the earliest idle time. This facilitates destination discovery, as the sender will also switch to the channel with the earliest idle time. Second, load balancing is indirectly achieved, as idle destinations avoid busy channels. Both properties are achieved without exchanging control messages.

As an example, consider the topology of Fig. 5(b). Assume that destination E resides on f_1. Initially, E sets the idle time for all channels to t_{curr}. When the $A \rightarrow B$ transmission occupies f_1, node E decodes BCN_B because it is a hidden terminal to A. Node E updates the idle time for f_1 to t_{ACK} and switches to f_2, because f_2 has the earliest idle time (ties are broken arbitrarily). Assume that transmission $C \rightarrow D$ is ongoing on f_2 when E switches to f_2. Node E cannot decode BCN_D since it is in the TO region. Node E uses the the worst-case estimate for the idle time of f_2 and sets the idle time to $t_{curr} + T_{MTU}$. It then switches to f_3 which is currently idle.

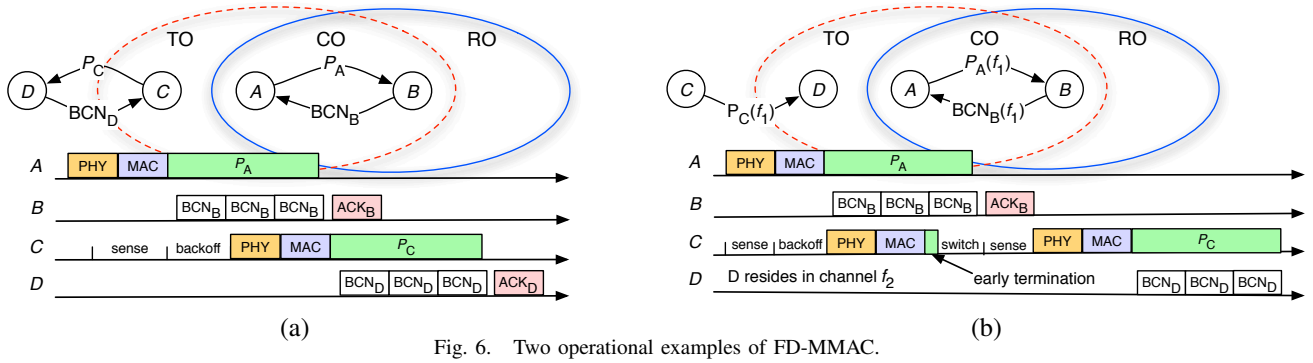

Fig. 6. Two operational examples of FD-MMAC.

B. Sender Operation

In FD-MMAC, we adapt the CSMA backoff mechanism to the multi-channel environment to reduce packet delay and achieve fairness. Referring to the state diagram of Fig. 5(c), a sender operates as follows.

Sense state: In the "Sense" state, the sender senses its resident channel f_i. If f_i is idle, it transitions to the "Backoff" state. If f_i is busy, it classifies its operation state using the region classification rules of Section IV. If the sender is in the TO region (exposed terminal), it transitions to the "Backoff" state. Otherwise, it transitions to the "Switch" state.

Backoff state: In the "Backoff" state, the sender selects a backoff value β for a packet P, by using the following rules:

1) In the first transition to the "Backoff" state for P, the sender draws β uniformly from $[0, cw_0]$, where cw_0 is the minimum contention window.
2) In any following transition from the "Sense" state, the sender retains the current β value (backoff is resumed from the current value).
3) In a transition from the "Wait ACK" state, the sender doubles the contention window and draws β uniformly (the contention window is capped at $cw_{\max}$).

In the "Backoff" state, the sender decrements β by one unit with every "idle" slot. Here, a slot is assumed to be idle if: (a) no channel activity is detected, or (b) the channel is busy but the sender is in the TO region. When $\beta = 0$, the sender transitions to the "Transmit" state. If the channel becomes busy before $\beta = 0$ (and the sender is not in the TO region), the sender transitions to the "Switch" state and freezes β.

Transmit state: In the "Transmit" state, the sender initiates the transmission of P. If the destination responds with a BCN packet, the sender continues the transmission of P. With the completion of P's transmission, the sender transitions to the 'Wait ACK" state. If a BCN is not detected, the sender aborts the transmission of P and transitions to the "Switch" state.

Wait ACK state: With the completion of P's transmission, the sender waits for an ACK by the destination. The sender transitions to the "Backoff" state if an ACK is not received by the expiration of the ACK timer, without transitioning to the "Switch" state. This is because the sender is aware that the destination resides on the current channel due to the reception of the BCN during the "Transmit" state. If the ACK reception is successful, the sender transitions to the "Switch" state.

Switch state: In the "Switch" state, the sender performs two operations. First, it updates the CST information and second, it decides on the next channel using the same switching rules as the destination. The CST is updated using the following rules:

1) If the sender is in the RO region of a transmission on f_i (BCN is decodable), it sets the idle time of f_i to t_{ACK}
2) If the sender is in the CO/TO region of a transmission on f_i (BCN is not decodable), it sets the idle time of f_i to $t_{curr} + T_{MTU}$.
3) If a sender transmitted a packet P on f_i, but did not receive a BCN response it sets the idle time of f_i to $t_{curr} + T_{MTU}$. This update leads to a channel switch to continue the destination discovery process.

Once the CST has been updated, the sender switches to the channel with the earliest idle time. Ties are broken arbitrarily.

C. FD-MMAC Operational examples

In Fig. 6, we present two operational examples for FD-MMAC. In the example of Fig. 6(a), node C has a packet for D while being in the TO region of the $A \rightarrow B$ transmission. Node C determines that it is in the TO region and can operate as an exposed terminal. Node C transitions to the "Backoff" state, selects β, and starts the backoff countdown. When $\beta = 0$, node C transitions to the "Transmit" state. Node C transmits P_C and receives BCN_D from D. Node C detects BCN_D using the signal correlation technique and continues the transmission of P_C. Upon termination of the P_A transmission, B transmits ACK_B which is detected at A using the signal correlation technique. Upon termination of the P_C transmission, D replies with ACK_D which is decodable at C.

In the example of Fig. 6(b), node A communicates with B at f_1. Node D switches from f_1 to f_2 to be available for packet reception. Node C, who resides on f_1, has a packet P_C for D. Initially, D is in the "Sense" state. Since f_1 is idle from C's perspective, C transitions to the "Backoff" state and selects a β. When $\beta = 0$, node C transitions to the "Transmit" state and starts the transmission of P_C. Because D resides on f_2, node C does not receive BCN_D. Node C transitions to the "Switch" state and updates the idle time for f_1 to $t_{curr} + T_{MTU}$. Based on the CST entries, C switches to f_2 which has the earliest idle time and transitions to the "Sense" state. Since f_2 is idle, C transitions to the "Backoff" state for a second time and retains $\beta = 0$. It then completes the communication with D.

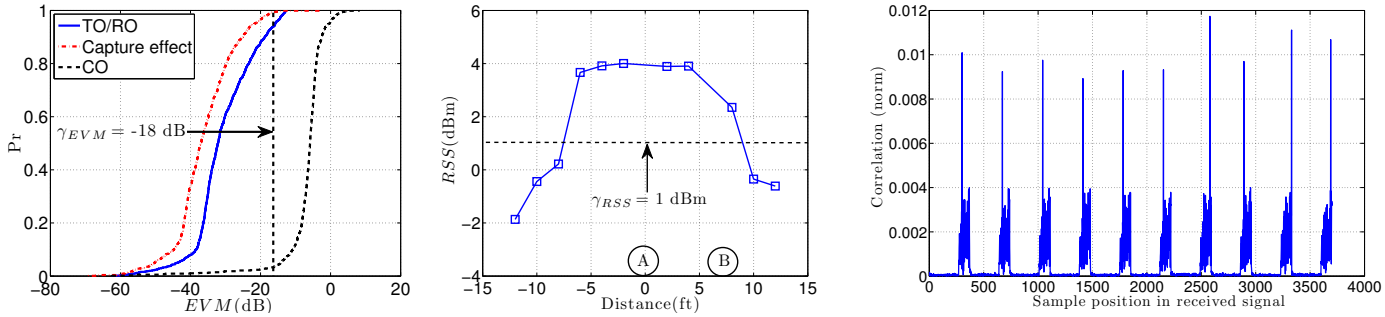

(a) (b) (c)

Fig. 7. (a) The EVM CDF at the RO, CO, and TO regions, (b) average RSS at different positions, (c) normalized correlation values for 10 BCN packets.

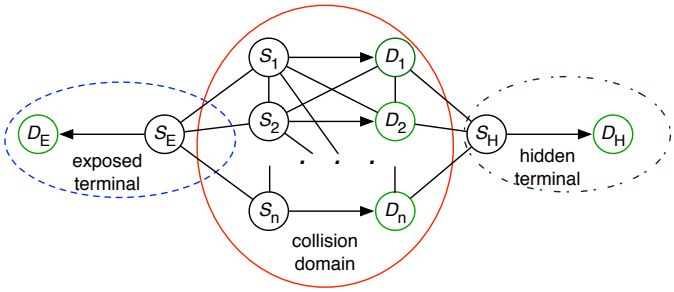

Fig. 8. The network topology used in the simulation experiments.

VII. Testbed Experiments and Simulations

In this section, we experimentally verify the PHY-layer techniques used by FD-MMAC and compare its performance with prior art via packet-level simulations.

A. Experimental Evaluation

Testbed: We performed our experiments on NI USRPs devices [25], over the 2.4 GHz band. The signal processing blocks were implemented in Labview [25]. Transmissions were modulated using the Quadrature Phase Shift Keying (QPSK) scheme at a transmission rate of 2Mbps. The radios applied phase/frequency offset correction and time synchronization using 88-bit preamble sequences.

Operation State Classification: To validate the operation state classification rules presented in Section IV, we replicated the topology of Fig. 3. Nodes A and B were placed 7ft apart and transmitted concurrently. Node A transmitted 100 P packets carrying a 500-bit payload, while node B transmitted 500 BCN packets with a 50-bit payload. We placed node C at positions $C_1, \ldots, C_4$ of Fig. 3 and measured the EVM, RSS, and the decodability of BCNs.

Fig. 7(a) shows the CDF of the EVM for the RO/TO region (positions C_1 and C_4), the CO region (position C_3), and position C_2 in the CO region. The RO and TO curves were averaged since they yielded very similar values. We observe that the EVM in the CO region (position C_3) is significantly higher compared with all other locations due to the collision of P with the BCN. The difference allows us to select the threshold γ_{EVM} for the EVM classification rule. In our experiments, we set $\gamma_{EVM} = -18$ dB to achieve a false positive rate of 2% ($EVM < \gamma_{EVM}$ when in the CO region) and a false negative rate of 4% ($EVM \geq \gamma_{EVM}$ when in the TO/RO region).

For position C_2, $EVM < \gamma_{EVM}$ due to the capture effect [24]. To avoid the classification of a node located at C_2 as an exposed terminal, we use the mean RSS value. Fig. 7(b) shows the mean RSS value for different receiver locations, averaged over the experiment duration. Nodes A and B were placed at positions 0ft and 7ft, respectively. For the RSS classification rule, we set γ_{RSS} to 1dBm. We observe that for location C_2 (within 2ft from A), C has an RSS value significantly higher than γ_{RSS}, and therefore infers that it is located in the CO region, despite having an $EVM < \gamma_{EVM}$. Also, for exposed terminal locations (more than 5ft from A), the EVM and RSS are below γ_{EVM} and γ_{RSS}, respectively.

Finally, we measured the fraction of BCN packets that can be decoded by C over ten repeated experiments (500 BCN packets each run). We recorded zero decodable BCN packets at locations C_1, C_2, and C_3, while 100% of the BCN packets were recovered at position C_4. We also placed C in the vicinity of B but within the CO. For this position, C was able to decode a large fraction of BCN packets due to the capture effect and falsely assume it is in the RO region. However, this error does not impact the correct FD-MMAC operation because, for all practical purposes, a node in the RO region defers from transmission similar to a node in the CO region.

Signal Correlation: We experimentally evaluated the signal correlation technique for the exposed terminal topology of Fig. 4(b). Node A transmitted 500-bit long data packets continuously while node D transmitted 50-bit long BCN packets. Node C applied the signal correlation method to detect BCN_D packets. Fig. 7(c) shows the normalized correlation [25] for a snapshot of ten BCN packets, when C is placed between A and D, at a 7ft distance from each. The correlation peaks correspond to the BCN transmissions and can be clearly distinguished. In our experiments, we set the detection threshold to 0.005. We placed C in three discrete positions between A and D to replicate the exposed terminal topology and measured the percentage of BCN_D packets that can be detected by correlating the received signal with the known BCN pattern (preamble + payload). Node D transmitted 1,000 BCN packets. The results are shown in Table 2. Distances are measured from node D.

Table 2: Fraction of Detected BCN Packets

Distance from D	3 ft	5 ft	7 ft
Percentage	100%	99%	94%

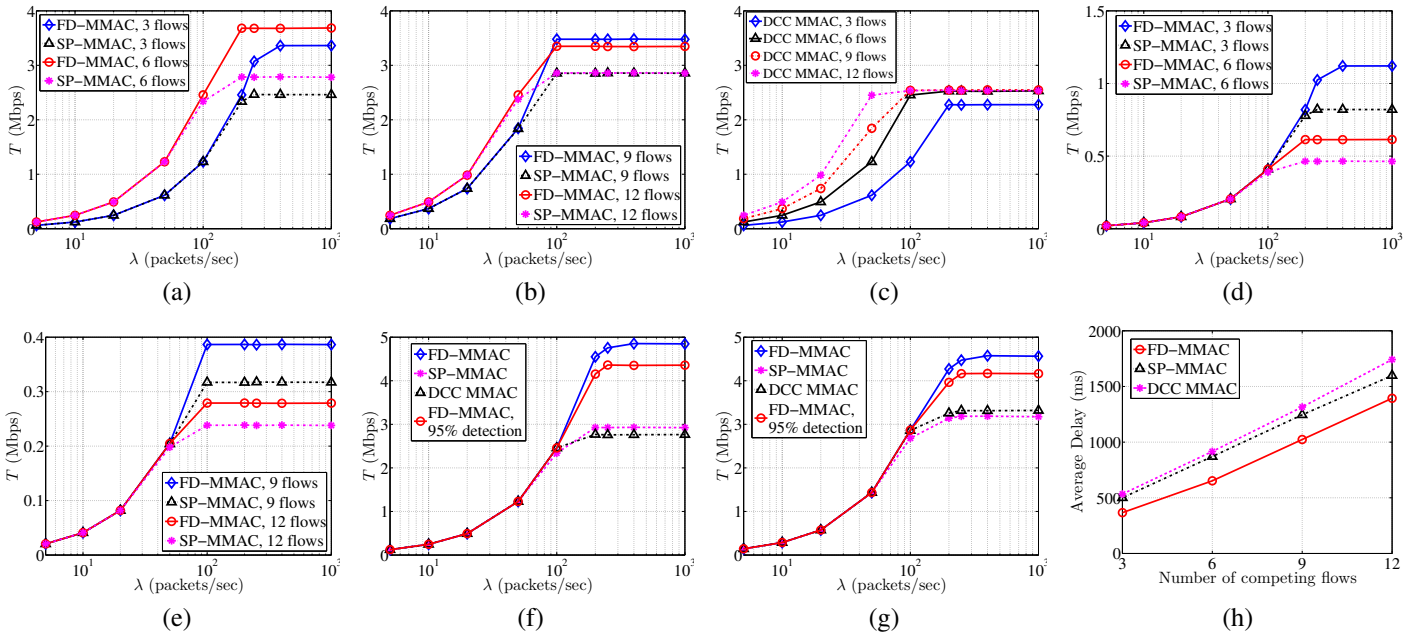

Fig. 9. (a),(b),(c) Aggregate T of FD-MMAC, SP-MMAC, and DCC MMAC when 3, 6, 9, and 12 flows are within same collision domain, (d),(e) per-flow average T for FD-MMAC and SP-MMAC when 3, 6, 9, and 12 flows are within same collision domain, (f) aggregate T in the presence of an exposed terminal, (g) aggregate T in the presence of one exposed and one hidden terminal, (h) average delay for transmitting a batch of 100 data packets.

Table 2 shows that a node in the collision domain of two transmitters can reliably detect a packet with known pseudo-random pattern using the signal correlation.

B. Simulated Experiments

Simulation Setup: We performed packet-level simulations using OPNET$^{\text{TM}}$ [26]. In our setup, multiple sender-destination pairs (flows) were organized in the topology of Fig. 8 and shared three orthogonal channels with 2Mbps capacity. For each sender, the arrival process at the MAC layer followed the Poisson distribution with parameter λ packets per second. Each packet was 512 bytes long. The channel switching delay was set to 20 μsec. Simulations were run for 40 sec and results were averaged over 20 simulation runs.

Throughput (T): In the first set of experiments, we compared the FD-MMAC throughput with the throughput of the split-phase MMAC (SP-MMAC) in [3] and of the DCC MMAC in [6]. The control and data phase of SP-MMAC were set to 20ms and 80ms, respectively [3]. Fig. 9(a), 9(b), and 9(c) compare the aggregate throughput for a varying number of contending flows, co-located in the same collision domain (senders S_E and S_H were idle). For low λ's, all protocols achieve similar throughput due to low contention. However, in saturation conditions, FD-MMAC achieves significantly higher aggregate throughput compared with the other protocols, due to the elimination of signaling for channel negotiation and virtual carrier sensing. Fig. 9(d) and 9(e) show the average per-flow throughput of FD-MMAC and SP-MMAC. FD-MMAC significantly outperforms SP-MMAC in saturation conditions.

In the second set of experiments, we placed five flows $S_1 \rightarrow D_1, \ldots, S_5 \rightarrow D_5$ in the same collision domain, while S_E operated as an exposed terminal to $S_1, \ldots, S_5$. For FD-MMAC, we considered two scenarios. In the first scenario, BCN and ACK packets were perfectly detected using the signal correlation technique. In the second scenario, 5% of BCNs and 5% of ACKs were undetectable by the intended recipients. From Fig. 9(f), we observe that in saturation conditions, FD-MMAC achieves an aggregate throughput that is 65% higher compared with SP-MMAC and 75% higher compared with DCC MMAC under ideal operating conditions. The throughput improvement drops to 49% and 58%, respectively, when 5% of BCN and ACK packets are assumed lost.

The superior performance of FD-MMAC is due to the parallel operation of S_E with any of the $S_1, \ldots, S_5$. In fact, the individual throughput of S_E was 51% higher than the throughput of $S_1, \ldots, S_5$ (1.12 Mbps for S_E vs. 0.74Mbps for each $S_1, \ldots, S_5$) because S_E did not contend with any other sender. On the other hand, for SP-MMAC and DCC MMAC, S_E operated in the same collision domain with $S_1, \ldots, S_5$ and its throughput dropped to 0.51Mbps and 0.68Mbps, respectively. Further, we evaluated the concurrent existence of exposed and hidden terminals. Five flows were placed in the same collision domain, S_E operated as an exposed terminal and S_H operated as a hidden terminal. Fig. 9(g) shows that FD-MMAC achieves 43% and 38% higher throughput in saturation conditions compared with SP-MMAC and DCC MMAC, respectively.

Delay: In the third set of experiments, we evaluated the packet delay for bursty packet arrivals. We loaded the transmission queue of each sender with 100 packets and measured the delay until all 100 packets were delivered to their respective destinations. All flows were within same collision domain. Fig. 9(h) shows the average delay as a function of the number of competing flows. We observe that FD-MMAC reduces the delay due to the elimination of the control message exchange before

packet transmissions. The delay increases almost linearly with the number of contending flows for all protocols, because the available channels are shared by more flows in a fair manner.

Fairness and Load Balancing: We also examined the fairness and load balancing properties of FD-MMAC under different traffic load conditions. To evaluate fairness, we use the Raj Jain's *Fairness Index* (FI):

$$FI = \frac{(\sum_{i=1}^{n} T_i)^2}{n \times \sum_{i=1}^{n} (T_i)^2} \quad (3)$$

where T_i is the throughput of the i^{th} flow and n is the total number of flows. The FI varied from 0.97 (for a topology with an exposed terminal present) to 0.999 (for a topology with six flows in the same collision domain), indicating that FD-MMAC achieves fair distribution of resources among competing flows. The FI is slightly smaller than one in the presence of an exposed terminal flow, because the exposed terminal node does not contend with other senders. We also evaluated the traffic load carried by each channel by computing the *Load Balancing Index* (LBI) in saturation conditions:

$$LBI = \frac{(\sum_{i=1}^{3} T_{f_i})^2}{3 \times \sum_{i=1}^{3} (T_{f_i})^2}, \quad (4)$$

where T_{f_i} is the aggregate throughput on channel f_i. The LBI value varied from 0.904 (for a topology with an exposed terminal) to 1 (for a topology with only three flows). The LBI value is lower than 1 under an exposed terminal topology because the same channel is concurrently occupied by two flows during an exposed terminal operation.

VIII. Conclusion

We proposed FD-MMAC, a distributed MMAC protocol that exploits FD communications to coordinate channel access at low control overhead. FD-MMAC eliminates control signaling for combating the multi-channel hidden terminal problem, discovering the resident channel of destinations, and performing load-balancing. Further, it increases the spatial channel reuse by enabling the operation of multi-channel exposed terminals. The FD-MMAC properties are achieved by utilizing an advanced suite of PHY-layer techniques, including SIS, EVM and RSS measurements, and signal correlation techniques. These techniques were experimentally validated on the NI USRP testbed and via simulations.

Acknowledgments

This research was supported in part by the NSF under grants CNS-0844111 and CNS-1016943 and ARO grant W911NF-13-1-0302. Any opinions, findings, conclusions, or recommendations expressed in this paper are those of the author(s) and do not necessarily reflect the views of the NSF.

References

[1] IEEE 802.11 Working Group. Wireless LAN medium access control (MAC) and physical layer (PHY) specifications. *IEEE 802.11 LAN Standards 2007*, 2007.

[2] P. Bahl, R. Chandra, and J. Dunagan. SSCH: slotted seeded channel hopping for capacity improvement in IEEE 802.11 ad-hoc wireless networks. In *Proc. of the MOBICOM Conference*, pages 216–230, 2004.

[3] J. So and N.H. Vaidya. Multi-channel MAC for ad hoc networks: handling multi-channel hidden terminals using a single transceiver. In *Proc. of the MOBIHOC Conference*, pages 222–233, 2004.

[4] T. Luo, M. Motani, and V. Srinivasan. Cooperative asynchronous multichannel MAC: Design, analysis, and implementation. *IEEE Trans. on Mobile Computing*, 8(3):338–352, 2009.

[5] J. Zhang, G. Zhou, C. Huang, S.H. Son, and J.A. Stankovic. TMMAC: An energy efficient multi-channel mac protocol for ad hoc networks. In *Proc. of the ICC Conference*, pages 3554–3561, 2007.

[6] S. L. Wu and J. Y. Yang. A novel channel assignment scheme for improving channel reuse efficiency in multi-channel ad hoc wireless networks. *Computer Communications*, 30(17):3416–3424, 2007.

[7] K. H. Almotairi and X. S. Shen. Multichannel medium access control for ad hoc wireless networks. *Wireless Communications and Mobile Computing*, pages 1–14, 2011.

[8] N. Jain, S.R. Das, and A. Nasipuri. A multichannel CSMA MAC protocol with receiver-based channel selection for multihop wireless networks. In *Proc. of the ICCCN Conference*, pages 432–439, 2001.

[9] T. Shu, S. Cui, and M. Krunz. Medium access control for multi-channel parallel transmission in cognitive radio networks. In *Proc. of the Globecomm Conference*, pages 1–5, 2006.

[10] X. Xing, K Liu, and H. Lu. A multichannel mac protocol to solve exposed terminal problem in multihop wireless networks. In *Proc. of the CCNC Conference*, pages 1–2, 2009.

[11] A. Sahai, G. Patel, and A. Sabharwal. Pushing the limits of full-duplex: Design and real-time implementation. Technical Report TREE1104, Rice University, February 2011.

[12] M. Jain, J. Choi, T. Kim, D. Bharadia, S. Seth, K. Srinivasan, P. Levis, S. Katti, and P. Sinha. Practical, real-time, full duplex wireless. In *Proc. of the MobiCom Conference*, pages 301–312, 2011.

[13] B. Radunovic, D. Gunawardena, P. Key, A. Proutiere, N. Singh, V. Balan, and G. Dejean. Rethinking indoor wireless mesh design: Low power, low frequency, full-duplex. In *IEEE Workshop on Wireless Mesh Networks*, pages 1–6, 2010.

[14] J. Choi, M. Jain, K. Srinivasan, P. Levis, and S. Katti. Achieving single channel, full duplex wireless communication. In *Proc. of the MobiCom Conference*, pages 1–12, 2010.

[15] S. Gollakota and D. Katabi. ZigZag decoding: combating hidden terminals in wireless networks. In *Proc. of the ACM SIGCOMM Conference*, pages 159–170, 2008.

[16] S. Liu, L. Lazos, and M. Krunz. Thwarting control-channel jamming attacks from inside jammers. *IEEE Trans. on Mobile Computing*, 11(9):1545–1558, 2012.

[17] A. Proano and L. Lazos. Selective jamming attacks in wireless networks. In *Proc. of the ICC Conference*, pages 1–6, 2010.

[18] J. Chen, S.T. Sheu, and C.A. Yang. A new multichannel access protocol for IEEE 802.11 ad hoc wireless LANs. In *Proc. of the PIMRC Conference*, volume 3, pages 2291–2296, 2003.

[19] W. So, J. Walrand, and J. Mo. McMAC: a parallel rendezvous multi-channel MAC protocol. In *Proc. of the WCNC Conference*, pages 334–339, 2007.

[20] A. Gupta, X. Lin, and R. Srikant. Low-complexity distributed scheduling algorithms for wireless networks. *IEEE/ACM Trans. on Networking (TON)*, 17(6):1846–1859, 2009.

[21] O. Simeone, U. Spagnolini, Y. Bar-Ness, and S. Strogatz. Distributed synchronization in wireless networks. *IEEE Signal Processing Magazine*, 25(5):81 –97, 2008.

[22] N. Singh, D. Gunawardena, A. Proutiere, B. Radunovic, H. Balan, and P. Key. Efficient and fair MAC for wireless networks with self-interference cancellation. In *In Proc. of the WiOpt Symposium*, pages 94–101, 2011.

[23] R. A. Shafik, S. Rahman, and R. Islam. On the extended relationships among EVM, BER and SNR as performance metrics. In *Proc. of the ICECE Conference*, pages 408–411, 2006.

[24] J. Lee, W. Kim, S. Lee, D. Jo, J. Ryu, T. Kwon, and Y. Choi. An experimental study on the capture effect in 802.11a networks. In *Proc. of ACM WiNTECH Conference*, pages 19–26, 2007.

[25] NI. National instruments. http://www.ni.com/usrp/, 2013.

[26] OPNET. OPNET technologies inc. http://www.opnet.com, 2009.